ADVANCED OPTICAL MATERIALS
www.advopticalmat.de

Enhanced Luminescence Characteristics of Remote Yellow Silicate Phosphors Printed on Nanoscale Surface-Roughened Glass Substrates for White Light-Emitting Diodes

*Jun Sik Kim, Senthil Kumar Eswaran, Oh Hyeon Kwon, Seung Jun Han, Joo Hong Lee, and Yong Soo Cho**

Nonconventional ways to modify phosphor structures have been reported to enhance the overall luminous efficacy of white light-emitting diodes (LED). Here, a nanoscale texturing technique of a glass substrate with the simple printing process of yellow $(Ba,Sr,Ca)_2SiO_4:Eu^{+2}$ silicate phosphor paste is combined to achieve enhanced white luminescence performance. It is demonstrated that the luminous efficacy of the resulting printed phosphor layer can be enhanced by ≈16% as a result of controlling surface roughness of the substrate up to 151 nm. The substantial improvement obtained by texturing both sides of the substrate is attributed to the reduction of total internal reflection of rays at the glass–air interface, combined with reduction of specular reflection at the phosphor–glass interface. For the surface-textured configuration, 3D ray tracing simulations reveal that more rays can be extracted with a widely scattered radiation pattern on the surface. Far-field luminance uniformity is also found to be significantly improved as a result of the texturing technique.

1. Introduction

Despite significant advancements in phosphor-converted white light-emitting diode (LED) technology, continuing studies on designing advanced LED structures have been reported for better luminescence and reliability.[1–6] The remote phosphor approach that minimizes the thermal degradation of phosphors and the absorption of re-emitted light by the LED chip has been regarded as one of the promising techniques.[7–9] Nonconventional ideas to enhance the luminescence performance of, specifically, the remote structure have been recently reported in various ways. They include new low-cost phosphor layers,[10–13] glass-involved phosphor pellets,[14,15] printing/coating techniques,[6,13,16] and new phosphor structures[17,18] for better performance of white LED structures. However, there have been limited improvements in luminous efficacy, which still remains a serious challenge hindering commercial success.

Trapped loss of light in the air-gap (due to backward photons) and total internal reflection (TIR) arising within the remote structure are the main factors that critically limit the light extraction.[19–21] The reported earlier methods such as scattered photon extraction[22] and diffused reflection cup approach[23] have mainly improved the extraction of back reflected light. By contrast, few studies to enhance the luminous efficacy by reducing the TIR in the phosphor part have been reported. Our approach in this study is to adopt a simple nanoscale surface roughening technique to enhance the luminous efficacy by minimizing the TIR at the air-phosphor layer and air–glass substrate interface of a remote phosphor LED consisting of yellow phosphor screen-printed on a glass substrate. In the past, surface roughening or surface texturing approaches have been applied to the top n-GaN layer of blue InGaN LED chips to enhance blue light emission by minimizing TIR at the semiconductor–air interface.[24–26] Notwithstanding the promising results of surface roughening methods, there have been very limited reports on the deployment of surface texturing techniques for the phosphor layer. One related report is about the random texturing in the case of yttrium aluminum garnet (YAG) phosphor by means of an imprint technique which resulted in an increased luminous flux by ≈5.4%.[27] A patterned YAG phosphor created by pulsed spray coating on a transparent silicone encapsulant resin using a circular mask was reported without increasing the luminous efficacy.[28]

In this work, we explore a simple surface roughening technique of the glass substrate used as a base for printable remote silicate phosphor, $(Ba,Sr,Ca)_2SiO_4:Eu^{2+}$, for the purpose of enhancing the luminescence performance. Compared to other YAG-based phosphors, this yellow silicate phosphor is known to possess higher luminous efficacy and to have advantages in commercial utilization and cost-effectiveness. We recently reported the utilization of a glass substrate for printable silicate

J. S. Kim, Dr. S. K. Eswaran, O. H. Kwon, Prof. Y. S. Cho
Department of Materials Science and Engineering
Yonsei University
Seoul 120-749, South Korea
E-mail: ycho@yonsei.ac.kr
J. S. Kim, S. J. Han, J. H. Lee
R&D Center
LG Display Co., Ltd
Gyeonggi-do 413-811, South Korea

DOI: 10.1002/adom.201500734

phosphors as an alternative remote phosphor approach, with a noticeable luminous efficacy of ≈32 lm W^{-1} at 200 mA, which depended on the firing temperature and position of printed phosphor layer.[13] The glass frit used as a matrix phase, which has a low-softening-temperature in the phosphor layer, provided solid adhesion and long-term stability. In the present work, we achieved a significant ≈16% improvement in luminous efficacy by introducing nanoscale roughness to the glass substrate prior to the printing process, by means of a simple scrubbing process. The utilization of this simple roughening technique for the printable remote phosphor layer has not been reported so far. This technique is assumed to be applicable for any other remote phosphor structure designed on the planar glass substrate.

2. Results and Discussion

Roughened soda-lime-silicate (SLS) glass substrates were analyzed by means of atomic force microscopy (AFM); their surface roughness varied from 20 to 151 nm depending on the grit size of the sandpaper used for the scrubbing process (**Figure 1**a). Although the surface texturing of the glass substrates is quite random, the creation of rough surfaces by means of this simple process may be beneficial because it can control surface reflection. Commercially available scrubbing techniques using sand paper or polishing (or roughening) media would likely be applicable for producing glass plates with rough surfaces. The glass substrate provides an anchoring base for the printed phosphor layer. When combined with the proper glass matrix used in the phosphor thick film, the glass substrate can be adhered very well with the softened glass matrix upon firing because the bonding is based on the interaction between glass and glass. The densified glass matrix is quite stable in terms of chemical reaction with embedded silicate phosphors as reported elsewhere.[13,29] Note that thermal degradation of regular resin-phosphor is coming from the chemical interaction of phosphors with the polymer resin in a conventional LED package.

Figure 1b schematically illustrates the processing steps used to fabricate a remote phosphor-based white LED structure consisting of yellow phosphor layer printed on the roughened glass substrate. The roughened surface can be applied to either or both sides of the substrate; the effects of each of the corresponding roughened configurations upon luminescence are discussed later. An example cross-sectional scanning electron microscope (SEM) image of the yellow silicate phosphor screen-printed on a surface-roughened substrate is shown in Figure 1c, including a magnified image of the roughened surface, which is of R_a = 151 nm. The screen printing process yielded a uniform phosphor layer with a thickness of ≈15–20 µm. The screen-printed phosphor layer consisted of yellow silicate phosphor particles embedded in a glass matrix. A low-softening glass frit of bismuth zinc silicates was used as the glass matrix. During firing at 410 °C, the glass frit softens at moderate temperatures and enables the thick film to be densified, yielding excellent adhesion with the substrate.[13] The phosphor layer is preferable to be positioned in the bottom because the luminous efficacy of the bottom-coated design was found to be better than the top-coated design.[13] Figure 1d shows cross-sectional images of the energy dispersive spectroscopy (EDS) mapping of Bi, Sr, and Si elements. Note that Bi is the main component of the glass frit used as a matrix phase, while Sr and Si are coming from the yellow silicate phosphor particles. It is evident that the phosphor particles are uniformly distributed over the glass matrix in the phosphor layer.

Dependence of the luminous efficacy upon the root mean square (rms) roughness R_a of the phosphor-coated glass substrates is plotted in **Figure 2**a. The roughness of 20 nm corresponds to the unroughened reference sample. The luminous efficacy increased gradually with increasing roughness of the glass substrate from ≈32 lm W^{-1} for the reference sample to ≈35.2 lm W^{-1} for the top-roughened sample with R_a = 151 nm.

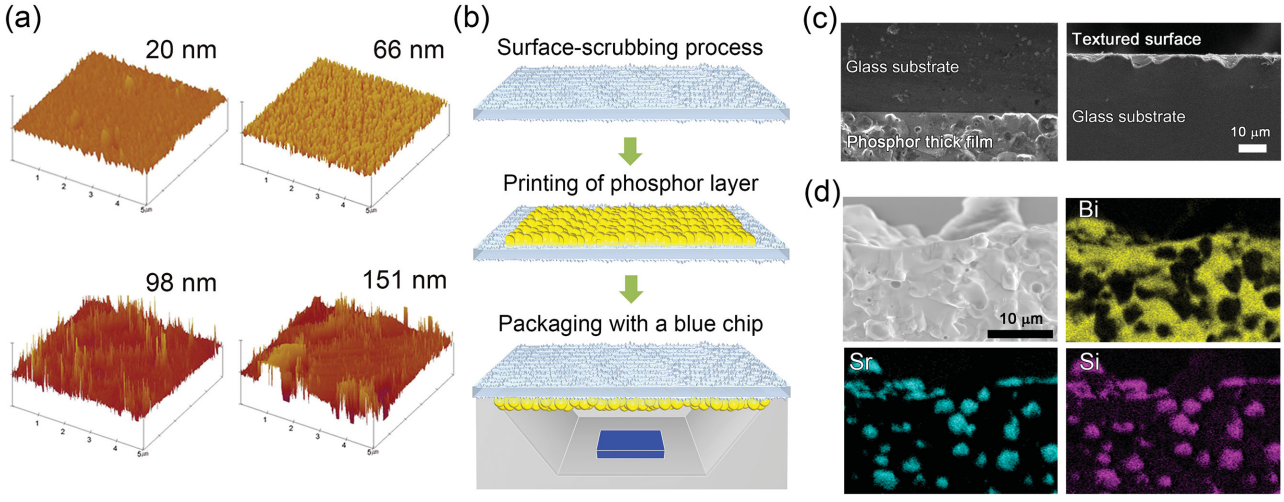

Figure 1. a) AFM images of flat and surface-textured SLS glass substrates of various surface roughnesses. b) Schematic illustration of the steps used to fabricate remote phosphor white LEDs based on blue LED chips and remote phosphors comprising yellow silicate phosphors embedded in a glass matrix, screen-printed onto surface-roughened glass substrates. c) SEM images of the silicate phosphor screen-printed on the glass substrate and magnified surface structure of roughness 151 nm. d) Elemental EDS mapping images of the Bi, Sr, and Si. Both the Sr and Si come from phosphor particles, whereas Bi is the main component of the glass frit.

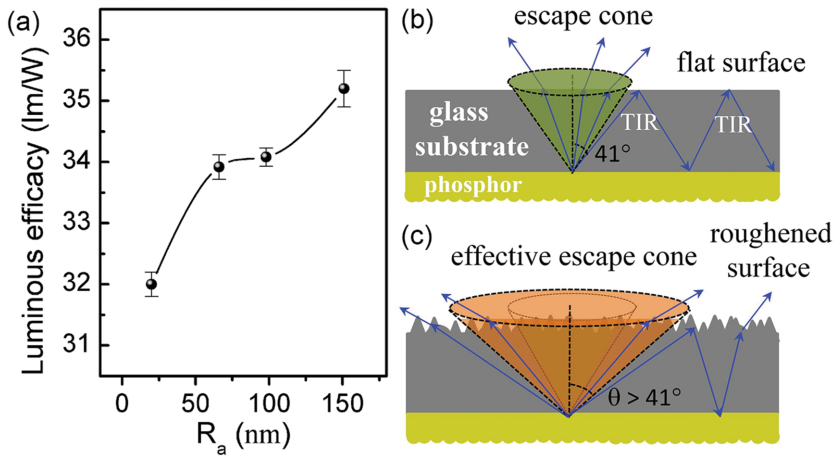

Figure 2. a) Dependence of the luminous efficacy upon the surface roughness of the SLS glass substrate. Schematic illustrations of the escape of white light from b) a flat surface and c) a roughened surface.

It is clear that the increasing dependence of efficacy with roughness is not linear: the efficacy was nearly maintained in the roughness range between ≈65 and ≈100 nm before a substantial increase with ≈150 nm roughness. The reason for the nonlinear dependence is not clear. It may be associated with the critical angle and the distribution of angles depending on surface roughness, which determine the levels of light reflection and extraction in this phosphor system. The estimated critical angle, $\theta_c = \sin^{-1}(n_{air}/n_{SLS})$,[24] for the white light to escape from the flat surface of SLS glass substrate was 41°, assuming that the refractive indices n_{SLS} and n_{air} were 1.523 and 1.0, respectively. Only those rays with angles of incidence less than 41° could escape the surface, as shown in the schematic of the flat surface in Figure 2b. Hence, the fraction of the white light escaping the flat surface, $f = 0.5\ (1 - \cos\theta_c)$, was calculated to be only 12.3%; the rest likely underwent TIR and became trapped within the substrate.[30]

On the other hand, the rays' escape probability from the surface-textured substrate is assumed to be greater than in the case of a flat surface. This is mainly because of angular randomization of rays by scattering from the roughened surface, which gives multiple opportunities for photons to find broader escape angle as depicted in Figure 2c.[31] The effective critical angle is expected to increase with increasing surface roughness because this broadens the range of incidence angles, ultimately increasing the volume of the effective light escape cone. Accordingly, a larger fraction of the white rays may escape the surface. Overall, the method of surface roughening of the SLS glass substrate is anticipated to reduce TIR, thereby enhancing the luminous efficacy. It should be mentioned that our simple scrubbing technique does not provide uniform texturing on the surface of substrate. If the uniform texturing is provided with careful control of critical angle θ_c, the luminescence efficiency is likely enhanced by minimizing TIR and thus by maximizing light extraction since the randomness means that some of incident light participates in the internal reflection.

The SLS glass substrate with the highest surface roughness of 151 nm was used in further investigations on the effect of the position(s) of roughened sides upon the light extraction performance. Four substrate configurations were used as shown in **Figure 3**a: a reference sample with no roughening, one with a roughened top side only, one with a roughened bottom side only, and one with both sides roughened; in all configurations, the phosphor layer was positioned on the bottom side. The dependence of luminance intensity upon the roughened surface configuration is plotted in Figure 3b. The relative luminance intensities of the bottom, top, and both sides configurations were 104%, 110%, and 116%, respectively.

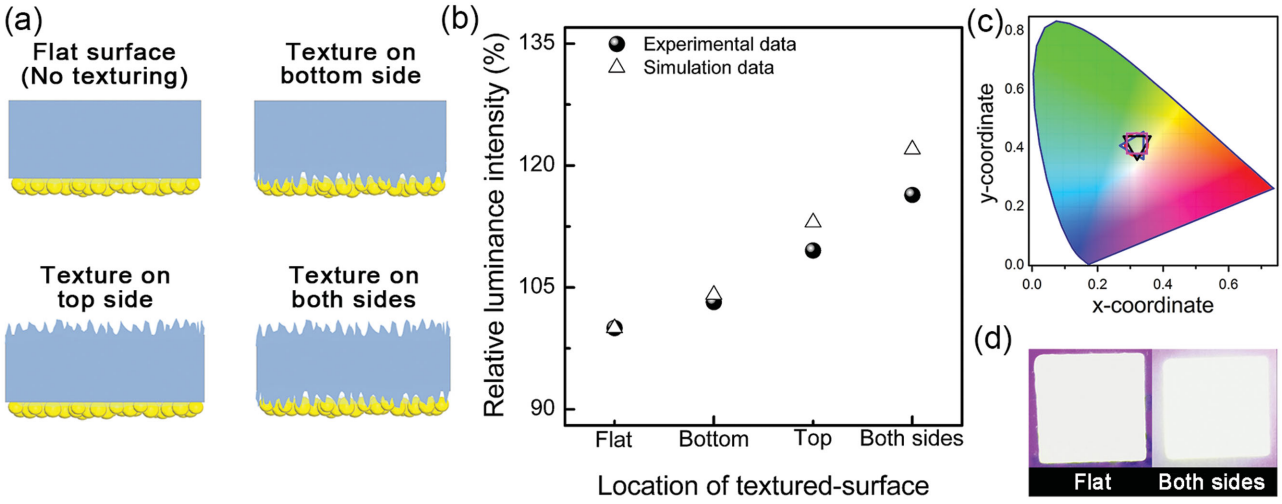

Figure 3. a) Schematic illustrations of four configurations of substrate: flat surface, bottom side textured, top side textured, and both side textured; with phosphor layer coating on bottom side for all the cases. b) Dependence of luminance (relative to the reference flat configuration) upon the configuration of roughened glass substrate surface(s). c) CIE color coordinates of remote phosphor LEDs with different textured surface configurations. d) Photographs of a remote phosphor LED with a flat glass substrate and one with a glass substrate roughened on both sides.

The both sides configuration yielded the highest luminous efficacy value of ≈37.1 lm W^{-1}, representing a 16% increase relative to the flat configuration. The achieved efficacy may be meaningful when considered to reported values for the similar yellow silicates.[32,33] The absolute values reported can not be directly compared with this case because the efficacy value is determined by the type and structure of phosphor and the input current and voltage values used for the luminescence measurement. It is believed that this current roughening technique is applicable for any other remote phosphor and brings a similar 16% increase in the luminous performance.

While we understand the effect of the position of roughened side, we need to consider also the glass substrate–air interface at the top surface and the phosphor–glass substrate interface at the bottom surface. As discussed above, surface roughening of the top surface minimizes the TIR and hence increases the luminance. However, the difference in refractive index between the phosphor glass matrix (≈1.43) and the SLS glass substrate (≈1.52) is small and hence the effect of TIR may not be significant at the bottom surface. However, surface roughening of the bottom glass substrate reduces the specular reflection of rays from the phosphor layer to the LED chip. Quantitatively, the intensity I_{Rs} of the specularly reflected rays at the bottom interface can be described as following[34]

$$I_{Rs} = I_{R0}\exp\left[-\left(\frac{2\sqrt{2\pi\sigma}}{\lambda}\cos\theta\right)^2\right] \quad (1)$$

where σ is the surface roughness, λ is the wavelength of light, and θ is the angle of incidence. I_{R0} is the intensity of the specularly reflected light when the surface roughness is zero. Since the phosphor was screen-printed onto the bottom surface of the glass substrate, the surface roughness of the glass substrate represents the interfacial roughness. From the above equation, it is evident that the intensity of specular reflection decreases with increasing surface roughness of the glass substrate/phosphor layer. For the bottom surface of roughness 151 nm, the intensity of the specularly reflected light decreased by six times relative to that of the flat surface. This promoted the diffusive transmission of light into the glass substrate. This is the reason why the bottom-phosphor configuration exhibited a higher luminance than the top-phosphor configuration. However, for the bottom configuration, although more rays were extracted from the phosphor into the glass substrate, the rays still underwent TIR at the top glass substrate–air interface. Hence, the both sides configuration helped further the extraction of light from the phosphor layer by reducing the specular reflection and concurrently by minimizing the TIR at the top surface, and hence resulted in the highest luminance among the samples studied.

Simulation studies were performed using a Light Tools optical simulation software package (Optical Research Associates) to evaluate the luminance intensity as also plotted in Figure 3b (open triangles). The trends in luminance variation matched well between the simulated and measured luminances, but the simulated luminance magnitudes tended to deviate from the measured values more largely for the configurations with greater luminance. This simulation technique may not reflect all light losses in the actual devices. Lee et al. also reported a similar dependence of light extraction efficiency on the position of surface texturing in a GaN blue LED as a result of Monte Carlo simulation.[35]

The International Commission on Illumination (CIE) chromaticity system is the method most commonly used to describe color compositions in terms of three primaries; CIE color coordinates were measured for LEDs of each of the surface configurations. Quite remarkably, the color coordinates were highly stable, independent of the surface roughness and the roughened surface configuration (Figure 3c). The color coordinates for the both sides configuration were (0.320, 0.416), very close to those of the reference surface, (0.319 and 0.412). This clearly indicates that surface roughening of the glass substrate enhances the light extraction efficiency without affecting the color coordinates of the white LED. Actual photographs of remote phosphor LEDs incorporating the flat and both sides configurations are shown in Figure 3d. The substrate roughened on both sides very clearly yielded brighter white emission than the flat substrate.

To further understand the effect of substrate roughening upon the light extraction of the remote phosphor LED, we performed 3D ray tracing simulations based on Snell's law, using the Light Tools optical simulation software. The mold and the chip were assumed to have the surface reflectances of 97% and 50%, respectively. The total number of traced rays was ≈10^6, including both blue (443 nm) and yellow (567 nm) light sources. **Figure 4**a–d shows the 3D ray tracing simulation results of the remote phosphor LED with the corresponding four configurations, respectively. The simulation results indicate that the level of ray scapes from the remote layer depends on the position of the applied surface roughness. The case of both sides-roughened surfaces showed the largest number of rays (Figure 4d). As discussed earlier, the differences are due to the broader range of light escape angles and hence the reduced chances of TIR, which are determined by the position and level of roughness. The results also support that the roughening on the top side is much effective in reducing specular reflection than the case of bottom side. In addition, distributions of light escaping from the LEDs with various roughness configurations were simulated as presented in Figure 4e–h. Inner and outer radiation rings were observed, and were associated respectively with the direct and reflected rays. The distribution pattern for the flat sample was very narrow with perfectly circular symmetry, likely due to the significant TIR and small light escape angle (Figure 4e). By contrast, size of the radiation pattern was spread over by applying the roughening technique as demonstrated in Figure 4f–h. It is worth noting that for the both sides case exhibited an irregularly scattered radiation pattern with an extensive light intensity distribution over the surface, which suggests a significant increase in the light escape area.

Far-field luminance uniformity of the remote phosphor LED samples with flat and both sides configurations were experimentally measured under the same input current conditions. The flat configuration produced a narrow light distribution around the center, which was attributed to its greater TIR and thus its narrower angles of light escape (**Figure 5**a). Contrastingly, the both sides configuration produced a wider, more uniform distribution of light (Figure 5b). The far-field luminance was plotted along the vertical and horizontal directions; for both

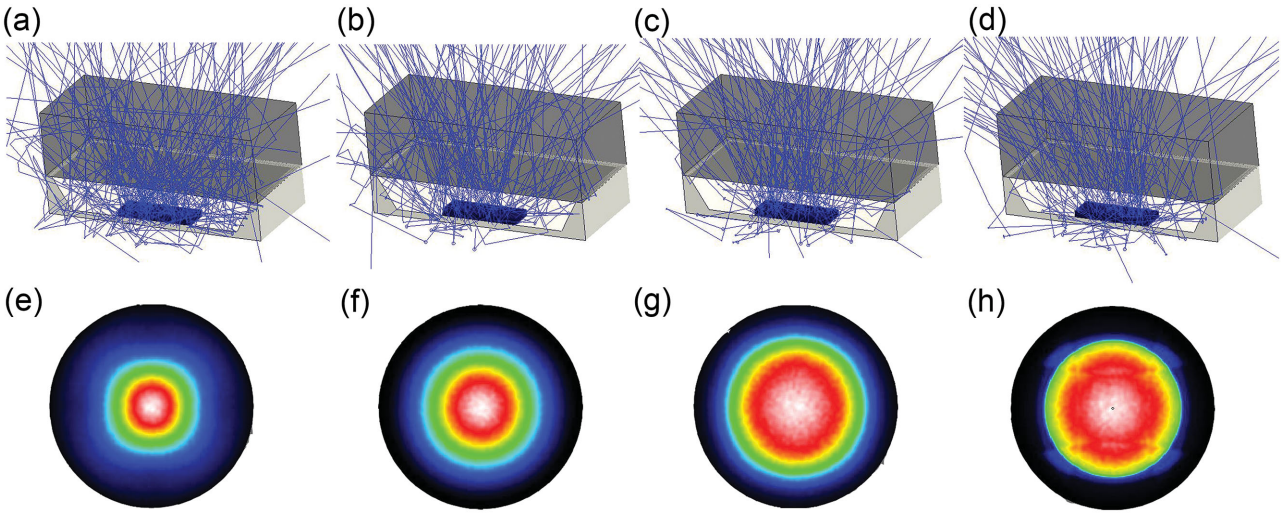

Figure 4. Simulated 3D ray tracing of the remote phosphor LED using a) flat surface, b) bottom side textured, c) top side textured, and d) both side textured glass substrates; e–h) corresponding light distributions.

configurations, luminance varied slightly along the vertical and horizontal directions with increasing distance from the center (Figures 5c,d). However, the luminance of the sample with the both sides configuration was greater in all directions than that of the flat configuration. The luminance plot was integrated to compute luminous efficiency. The result was identically a ≈16% improvement in the efficiency with the both sides configuration.

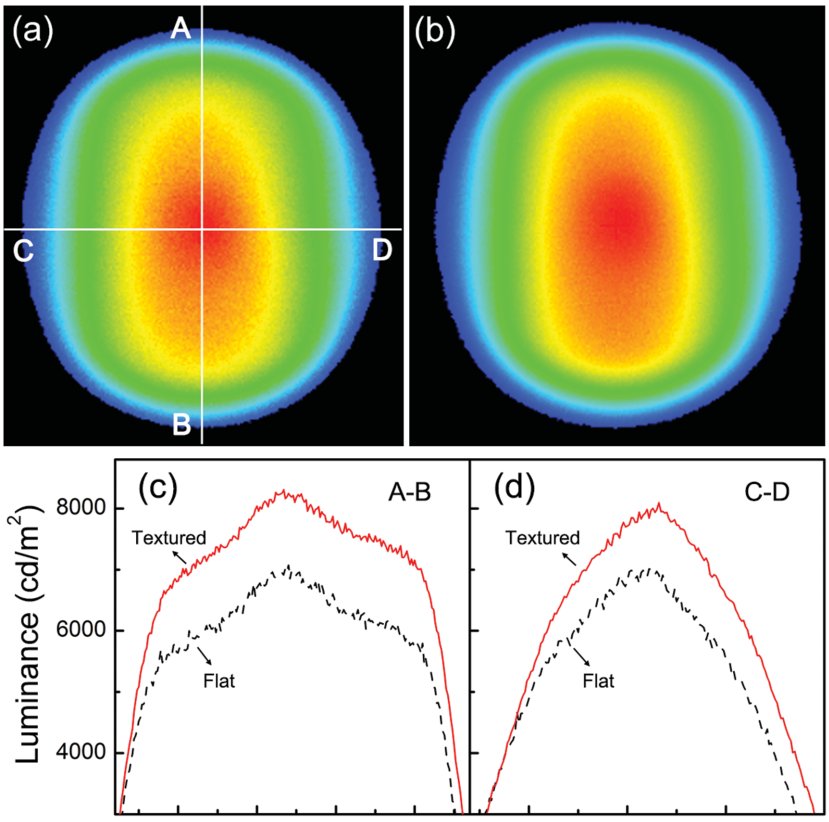

Figure 5. a,b) Far-field luminance uniformity of remote phosphors excited by a 443 nm blue LED at 443 nm excitation, of two different substrate roughness configurations: (a) flat surfaces, (b) substrate roughened on both sides. Luminance profiles along c) the vertical line A–B and d) the horizontal line C–D (solid red lines: textured surfaces; dotted lines: flat surfaces).

3. Conclusions

We have successfully demonstrated the use of nanoscale surface roughening method for a remote phosphor LED structure to improve the luminous efficacy. The resulting LED structure with yellow silicate phosphor screen-printed on a 151 nm surface-roughened glass substrate exhibited an enhanced luminous efficacy by ≈16% compared to the reference flat surface. The degree of enhancement depended on the level of roughness and the position of roughened surface. These results were in good agreement with the 3D ray tracing simulation that showed a relatively large amount of light escape with a wider range of scattered radiation pattern at the surface. A wider distribution and a relatively larger magnitude in the measured far-field luminance uniformity were confirmed as an origin of the enhancements from the surface-texturing technique.

4. Experimental Section

Surface Roughening and Printing Process: Prior to the printing process, the surfaces of SLS substrates (20 mm × 20 mm) were abraded using silicon carbide sand papers with different grit sizes (#220, 400, and 600). The scrubbing procedure of the substrate allowed us to control surface roughness in the range of 20–151 nm. After the scrubbing procedure, the substrate was ultrasonicated to remove the glass impurities. A yellow silicate phosphor $(Ba,Sr,Ca)_2SiO_4:Eu^{2+}$ (PA556, Force4 Co., Korea) was selected to prepare a composite-type phosphor layer with dispersion of the phosphor particles within a glass matrix. A commercially available Bi_2O_3-ZnO-B_2O_3 glass frit (BSP718, DAION Co., Incheon, Korea) with a softening point of ≈385 °C and an average particle size of ≈2.7 μm was used. The relative ratio of phosphor to glass frit was fixed at 40 wt%. The detailed procedure for paste fabrication was described in our previous work.[13] Viscous ink paste was prepared by admixing the glass frit and silicate phosphor with an organic vehicle composed of ethyl cellulose, α-terpineol and lauric acid at 1400 rpm for ≈6 min by using a paste mixer. The resultant paste with a viscosity of ≈150 cps was printed two to three times on the surface-roughened glass substrate by manual operation. The printed paste was dried at 120 °C for 1 h and then fired at a temperature of 410 °C for 30 min.

Effects of the relative content of phosphor in the phosphor/glass layers printed on a flat glass substrate are described in terms of microstructure and luminescence properties with Figures S1–S3 of the Supporting Information. The luminous efficacy of the samples increased substantially with increasing the relative content of phosphors from 20 to 70 wt%. The value reached ≈60.4 lm W^{-1} for the 70 wt% phosphor case. However, the variations in the CIE color coordinates in Figure S2 (Supporting Information) indicate the significant deviations from the white emission region, depending on the content of phosphor. Accordingly, the relative content of phosphor to glass frit was fixed as 40 wt%. All related luminescence values are listed in Table S1.

Characterization and Measurement: Surface and cross-sectional microstructures of the printed phosphor layer were observed by field emission scanning electron microscopy (FESEM: JEOL, JSM-5400, USA). Prior to screen-printing of the phosphor paste, surface roughness of the substrate was measured by means of tapping-mode AFM (Digital Instruments, Nanoscope IIId), conducted in air at room temperature using an Al back-coated Si cantilever. Luminescence properties were obtained using an integrating sphere system (ISP 1000, Instrument systems, Germany), and Commission Internationale de l'Eclairage (CIE) chromaticity coordinates were measured in a 1° measurement field of view by a colorimeter (PR-650: Photo Research, USA) using a 443 nm blue LED as an excitation source. The luminous efficacy η was calculated by a simple relationship of $\eta = L/P_{input}$, where L is the luminous flux (lumens) and P_{input} is the input power of the blue chip. Far-field luminance uniformity profiles of phosphor layers coated on the surface-textured glass substrate were investigated using a 2D luminance/color analyzer (CA-2000: Konica Minolta, Japan).

Supporting Information

Supporting Information is available from the Wiley Online Library or from the author.

Acknowledgements

J.S.K. and S.K.E. contributed equally to this work. This work was financially supported by a grant from the National Research Foundation of Korea (NRF-2013R1A2A2A01016711).

Received: December 8, 2015
Revised: January 31, 2016
Published online: March 17, 2016

[1] P. Pust, P. J. Schmidt, W. Schnick, *Nat. Mater.* **2015**, *14*, 454.
[2] C. J. Humphreys, *MRS Bull.* **2008**, *33*, 459.
[3] J. S. Lee, P. Arunkumar, S. Kim, I. J. Lee, H. Lee, W. B. Im, *Opt. Lett.* **2014**, *39*, 762.
[4] P. Acuna, S. Leyre, J. Audenaert, Y. Meuret, G. Deconinck, P. Hanselaer, *Opt. Exp.* **2014**, *22*, A1079.
[5] Y. Zhu, N. Narendran, *Jpn. J. Appl. Phys.* **2010**, *49*, 100203.
[6] S. Ye, F. Xiao, Y. X. Pan, Y. Y. Ma, Q. Y. Zhang, *Mater. Sci. Eng., R* **2010**, *71*, 1.
[7] M. T. Lin, S. P. Ying, M. Y. Lin, K. Y. Tai, S. C. Tai, C. H. Liu, J. C. Chen, C. C. Sun, *IEEE Photonics Technol. Lett.* **2010**, *22*, 574.
[8] Y. C. Lin, Y. Zhou, N. T. Tran, F. G. Shi, in *Materials for Advanced Packaging* (Eds: L. Daniel, C. P. Wang) Springer, New York **2009**.
[9] W. Peng, S. Jun, T. Hua, L. Q. Fei, W. D. Jian, *Optoelectron. Lett.* **2012**, *8*, 201.
[10] J. W. Jang, J. S. Kim, O. H. Kwon, T. H. Lee, Y. S. Cho, *Opt. Lett.* **2015**, *40*, 3723.
[11] A. A. Settlur, *Electrochem. Soc. Interfaces* **2009**, *18*, 32.
[12] P. Pust, V. Weiler, C. Hecht, A. Tucks, A. S. Wochnik, A. K. Hens, D. Wiechert, C. Scheu, P. J. Schmidt, W. Schnick, *Nat. Mater.* **2014**, *13*, 891.
[13] J. S. Kim, O. H. Kwon, J. W. Jang, S. H. Lee, S. J. Han, J. H. Lee, Y. S. Cho, *ACS Comb. Sci.* **2015**, *17*, 234.
[14] X. Zhang, L. Huang, F. Pan, M. Wu, J. Wang, Y. Chen, Q. Su, *ACS Appl. Mater. Interfaces* **2014**, *6*, 2709.
[15] X. Zhang, J. Wang, L. Huang, F. Pan, Y. Chen, B. Lei, M. Peng, M. Wu, *ACS Appl. Mater. Interfaces* **2015**, *7*, 10044.
[16] J. Burgin, V. Jubera, H. Debeda, B. Glorieux, A. Garicia, C. Lucat, *J. Mater. Sci.* **2011**, *46*, 2235.
[17] Z. Liu, S. Liu, K. Wang, X. Luo, *IEEE Trans. Mater. Reliab.* **2009**, *9*, 65.
[18] J. H. Hwang, Y. D. Kim, J. W. Kim, S. J. Jung, H. K. Kwon, T. H. Oh, *Phys. Status Solidi C* **2010**, *7*, 2157.
[19] H. Xiao, Y. J. Lu, T. M. Shih, L. H. Zhu, S. Q. Lin, P. J. Pagni, Z. Chen, *IEEE Photonics J.* **2014**, *6*, 8200108.
[20] S. C. Allen, A. J. Steckl, *Appl. Phys. Lett.* **2008**, *92*, 143309.
[21] S. P. Ying, A. Y. Shiu, *Appl. Opt.* **2015**, *54*, E30.
[22] N. Narendran, Y. Gu, J. P. Freyssinier-Nova, Y. Zhu, *Phys. Status Solidi A* **2005**, *202*, R60.

[23] J. K. Kim, H. Luo, E. F. Schubert, J. Cho, C. Sone, Y. Park, *Jpn. J. Appl. Phys.* **2005**, *44*, L649.
[24] J. H. Son, J. U. Kim, Y. H. Song, B. J. Kim, C. J. Ryu, J. L. Lee, *Adv. Mater.* **2012**, *24*, 2259.
[25] T. Fujii, Y. Gao, R. Sharma, E. L. Hu, S. P. DenBaars, S. Nakamura, *Appl. Phys. Lett.* **2004**, *84*, 855.
[26] S. J. Wang, K. M. Uang, S. L. Chen, Y. C. Yang, S. C. Chang, T. M. Chen, C. H. Chen, *Appl. Phys. Lett.* **2005**, *87*, 011111.
[27] H. C. Chen, K. J. Chen, C. H. Wang, C. C. Lin, C .C. Yeh, H. H. Tsai, M. H. Shih, H. C. Kuo, T. C. Lu, *Nanoscale Res. Lett.* **2012**, *7*, 188.
[28] H. C. Kuo, C. W. Hung, H. C. Chen, K. J. Chen, C. H. Wang, C. W. Sher, C. C. Yeh, C. C. Lin, C. H. Chen, Y. J. Cheng, *Opt. Express* **2011**, *19*, A930.
[29] X. Zhang, J. Yu, J. Wang, C. Zhu, J. Zhang, R. Zou, B. Lei, Y. Liu, M. Wu, *ACS Appl. Mater. Interfaces* **2015**, *7*, 28122.
[30] M. H. Shin, H. G. Hong, H. J. Kim, Y. J. Kim, *Appl. Phys. Expr.* **2014**, *7*, 052101.
[31] I. Schnitzer, E. Yablonovitch, C. Caneau, T. J. Gmitter, A. Scherer, *Appl. Phys. Lett.* **1993**, *63*, 2174.
[32] J. K. Park, C. H. Kim, S. H. Park, H. D. Park, *Appl. Phys. Lett.* **2004**, *84*, 1647.
[33] H. S. Jang, D. Y. Jeon, *Appl. Phys. Lett.* **2007**, *90*, 041906.
[34] R. K. Singh, Z. Chen, D. Kumar, K. Cho, M. Ollinger, *Appl. Surf. Sci.* **2002**, *197*, 321.
[35] T. X. Lee, C. Y. Lin, S. H. Ma, C. C. Sun, *Opt. Express* **2005**, *13*, 4175.